Supplementary Information (SI) for Physical Chemistry Chemical Physics.
This journal is © the Owner Societies 2025

Supporting Information

Defect physics investigations in bulk $NaBiO_3$ photocatalyst via Heyd-Scuseria-Ernzerhof hybrid density functional theory calculations

Song Ling [a], Jingcheng Wang [a,b], Bo Kong [a*], Ti-xian Zeng [c, d*], Wentao Wang [b*]

[a] School of Physics and Astronomy, China West Normal University, Nanchong 637002, China;

[b] Guizhou Provincial Key Laboratory of Computational Nano-Material Science, Guizhou Education University, Guiyang, 550018, China;

[c] College of Optoelectronic Technology, Chengdu University of Information Technology, Chengdu, 610225, China;

[d] Dazhou Industrial Technology Research Institute, Dazhou, 635000, China

E-mail: kongbo1108@cwnu.edu.cn (B. K.); zengtxnc@163.com; wtwang@gznc.edu.cn (W. W.)

Note S1: The details for the HSE method and the determination process of the mixing parameter α in the present hybrid functional calculations

For the HSE hybrid functional calculations, the exchange-correlation energy of the HSE function is defined by $E_{XC}^{HSE} = \alpha E_X^{SR}(\mu) + (1 - \alpha)E_X^{PBE,SR}(\mu) + E_X^{PBE,LR}(\mu) + E_C^{PBE}$. In this function, SR and LR represent the short-range and long-range interaction between electrons, μ is the ratio of the SR and LR parts. The μ value is set as the default value of 0.2 $Å^{-1}$. The band gap of the semiconductor is usually sensitive to the value of the mixing parameter α. The fault value for the mixing parameter α in VASP code is 0.25. However, the fault value usually cannot produce the reasonable band gaps for many semiconductors. Then, the mixing parameter α needs to be adjusted to achieve the experimental band gap value. In defect physics calculations, this is a general process when the HSE hybrid function is applied[1-5].

The experimental bandgap value of $NaBiO_3$ is 2.6 eV[6], and we obtain the bandgap value by adjusting the mixing parameter α in the HSE calculations. The details are listed in **Table. S1**. In **Table. S1**, it is seen that when the Hartree-Fock mixing parameter α is set to 0.32, the calculated HSE band gap is 2.62 eV, the bandgap value is very close to the experimental bandgap 2.60 eV of $NaBiO_3$[6]. Therefore, 0.32 is adopted for the mixing parameter α in the present HSE calculations.

Table. S1. The band gap values of $NaBiO_3$ obtained by HSE calculations for different mixing parameters α in unit eV.

α	0.15	0.20	0.25	0.31	0.32	0.33	0.35
HSE band gap	1.75	2.01	2.25	2.57	2.62	2.66	2.75

Note S2: How to calculate the Ecorr in Eq. (1) from the VASP output.

The correction term E_{corr} in Eq. (1) originates from the necessity to address electrostatic artifacts introduced in periodic boundary conditions during defect calculations. This term ensures that the computed defect formation energies accurately reflect the isolated defect behavior rather than periodic artificial interactions. In periodic systems, the electrostatic potential from charged defects interacts with its periodic images and a compensating background charge to maintain neutrality. As derived in the FNV method of Freysoldt *et al*[7], the correction energy can be expressed as:

$$E_{corr} = E_q^{lat} - q\nabla_{\frac{q}{0}} \tag{S1}$$

where E_q^{lat} is the lattice energy component reflecting periodic electrostatics, q is the defect charge state, and $\nabla_{q/0}$ is the short-range potential.

$$E_q^{lat} = \int_{\Omega} d^3r\left[\frac{1}{2}\left[q_d(r) + n\right]\left[\tilde{V}_q^{lr}(r) - V_q^{lr}(r)\right] + nV_q^{lr}(r)\right] \tag{S2}$$

where $q_d(r)$ is the charge distribution of the defect, a key physical quantity that describes how the defect affects the surrounding electric field, n is to neutralize the background charge and is used to compensate for the non-neutral effect of the total charge in the periodic system to ensure the electrical neutrality of the system. $\tilde{V}_q^{lr}(r)$ is the reconciling part of the long-range potential for dealing with interactions arising from mirror charges in the periodic regime. $V_q^{lr}(r)$ is the original long-range potential, which represents the long-range Coulomb potential generated directly by the defect and its mirror charge.

$$\Delta_{q/0} = \frac{1}{\Omega}\int_{\Omega} d^3\mathbf{r}V_{q/0}^{sr}(\mathbf{r}) \tag{S3}$$

where $\Delta_{q/0}$ denotes the potential alignment correction term between the defect state q and the reference state 0. This correction term is used to remove the potential reference deviation between systems of different charge states and to ensure that the energies of

the different charge states are comparable. $V_{q/0}^{sr}(\mathbf{r})$ denotes the short-range potential, which specifically describes the interaction between the charge defect and the background charge on a local scale.

Note S3: Defect and carrier concentration calculation method

At infinite temperature, the excited electrons from the conduction band minimum (CBM) and excited holes from the valence band maximum (VBM) will always affect the position of the Fermi level. The concentrations of these thermally excited electrons (n_0) and holes (p_0) are given as shown in[8]

$$n_0 = \int_{E_g}^{\infty} f_e(E)\rho(E)dE \tag{S4}$$

$$p_0 = \int_{-\infty}^{0} f_h(E)\rho(E)dE \tag{S5}$$

where E_g is the material bandgap, $f_e(E)$ is the Fermi-Dirac distribution function, expressed as $f_e(E) = [\exp((E_F - E)/kT) + 1]^{-1}$, and $f_h(E) = 1 - f_e(E)$. k is the Boltzmann constant, $\rho(E)$ is the total density of states of the pure supercell, and T is the temperature.

Additionally, we used the SC-FERMI code to calculate the carrier concentration of defects in $NaBiO_3$ at different temperatures. The principle is to calculate the concentration of defect X with charge state q as:

$$[X]^q = N_x g_q exp\left(-\frac{E_f(D^q)}{k_B T}\right) \tag{S6}$$

where N_x is the defect density of the possible formation of the defect, g_q is the degeneracy of charge state q, E_f is the formation energy of defect D with charge state q, k_B is the Boltzmann constant, and T is the temperature. The entire equation is achieved by integrating the Fermi-Dirac function to calculate the concentration of electrons (n_0) and holes (p_0). Thus, defects with sufficiently low formation energies are produced only when conditions tend to equilibrate, usually occurring during high-temperature growth or annealing[9]. Finally, the charge neutrality condition in semiconductor systems can be expressed as:

$$n_0 - \sum_X \sum_q q\left[C_X^q\right] = p_0 \tag{S7}$$

where the equation includes the sum of donor and acceptor defects. C_X^q depends on a set of defect formation energies {Ef (Xq)} that vary with temperature T. The other terms in the equation also depend on E_F, and the equilibrium Fermi energy level positions (E_F), carrier concentrations, and defect concentrations that satisfy Eq. S1 and S4-S6) can be calculated given a finite temperature T and a certain atomic chemical potential. Once the temperature T and chemical growth environment are determined, the Fermi level, carrier, and charged defect concentrations are also determined under the charge neutrality condition. Additionally, due to simplification, the defect formation energy E_F (X_q) is fixed and determined at E_F=0 eV, which reduces the formation energy of positively charged defects and increases the formation energy of negatively charged defects, leading to a discrepancy between the increase in positively charged defect concentration and the decrease in negatively charged defect concentration, but does not affect the concentration of neutral defects.

From the defect formation energies and total density of states obtained from supercell HSE calculations, we can see the self-consistent Fermi level E_F (red dashed line) calculated using the SC-FERMI code and the equilibrium concentrations of carriers and charged defects in $NaBiO_3$ under different chemical potential conditions (A_{HSE}, B_{HSE}, C_{HSE}, D_{HSE}, E_{HSE}) as a function of temperature T in the range of 50 to 1000 K, as shown in **Fig. 4**. For simplicity, it is assumed that the defect formation energy, unit cell parameters, total density of states in the pristine crystal, and bandgap do not vary with T[8-10].

Note S4: The calculations of optical absorption spectrum

The optical process at a microscopic level is presented from the complex dielectric function $\varepsilon(\omega) = \varepsilon_1(\omega) + i\varepsilon_2(\omega)$. The imaginary part $\varepsilon_2(\omega)$ is determined using the formula via first-principles calculations (VASP code)[11]:

$$\varepsilon_2(\omega) = \frac{2\pi e^2}{\Omega\varepsilon_0} \sum_{k,v,c} \left|\left\langle \Psi_k^c \middle| \hat{u} \cdot r \middle| \Psi_k^v \right\rangle\right|^2 \delta\left(E_k^c - E_k^v - \hbar\omega\right) \tag{S8}$$

Where ω is the light frequency, Ψ_k^c and Ψ_k^v are, respectively, the conduction and valence band wave functions at the k space calculated within the HSE approach. The vector $\hat{u}$ points along the polarization of the incident electric field. The real part of the dielectric

functions is computed from $\varepsilon_2(\omega)$ using the Kramers–Kronig relation in the form

$$\varepsilon_1(\omega) = 1 + \frac{2}{\pi} p \int_0^{\infty} \frac{\omega' \varepsilon_2(\omega')}{\omega'^2 - \omega^2} d\omega' \quad \text{(S9)}$$

where p means the principal value of the integral. Then, the absorption coefficient $\alpha(\omega)$ of the material determines the nature of transition in semiconductors and can be calculated directly from the dielectric function:

$$\alpha(\omega) = \sqrt{2}\frac{\omega}{c}\left[\sqrt{\varepsilon_1^2(\omega) - \varepsilon_2^2(\omega)} - \varepsilon_1(\omega)\right]^{\frac{1}{2}} \quad \text{(S10)}$$

where c is the speed of light in a vacuum.

The data post processing is carried out via VASPKIT code[12].

Note S5: The convergence of defect formation energy for different supercell sizes, taking the calculation of Na_i^{1+} defect formation energy for an example

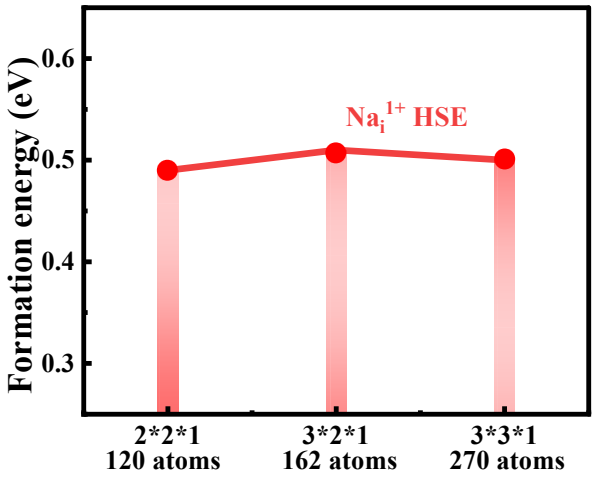

Fig. S1. The calculated HSE formation energies (eV) for Na_i^{1+} defect for different $NaBiO_3$ supercell sizes (120 atoms-2 × 2 × 1, 162 atoms-3 × 2 × 1, and 270 atoms-3 × 3 × 1 supercells) under oxygen-rich growth conditions with Fermi energy $E_F = 0$.

As shown in **Fig. S1,** the change in the Na_i^{1+} defect formation energy from 2×2×1 (120 atoms) to 3×3×1 (270 atoms) supercells is less than 0.1 eV, the defect formation energy of Na_i^{1+} converges at the adopted 2 × 2 × 1 supercell size.

Note S6: Charge state convergence Test in $NaBiO_3$

When the defect formation energy is calculated, each intrinsic defect may have different charge states, requiring a convergence test of the formation energy for different charge states. **Fig. S2** examines the formation energies of all considered intrinsic point defects in $NaBiO_3$ relative to the Fermi level, including all possible defect

charge states. Since different chemical potential growth conditions do not affect the formation energy changing trend of each defect with different charge valance states, we take the Bi-poor, Na-poor, and O-rich growth conditions at point A_{HSE} in the phase diagram **(Fig. 2)** as an example for the investigations.

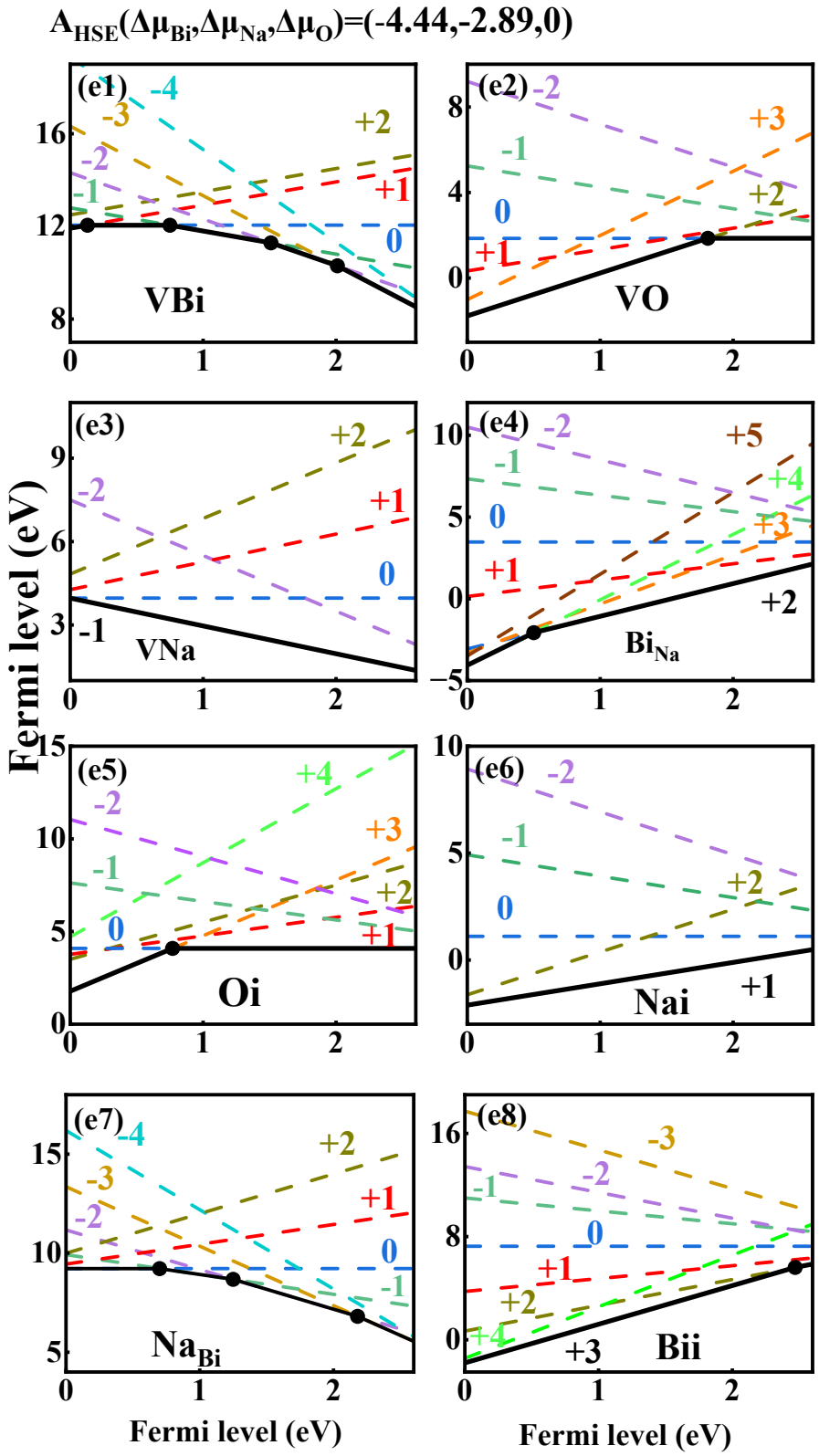

Fig. S2. Formation energies of 8 intrinsic point defects in $NaBiO_3$ as a function of the Fermi level relative to the VBM under Bi-poor, Na-poor, and O-rich growth conditions. Dashed lines represent the formation energies of defects at the corresponding charge states, and solid lines represent the lowest formation energy among all charge states. The Fermi levels at the VBM and CBM are set to be 0.00 eV and 2.62 eV, respectively.

For Bi vacancies as shown in **Fig. S2** (e1), considering the negative charge states, the corresponding formation energy in the -4 charge states is higher than those of all less negative charge states; and for positive charge states, the formation energy of the in the +2 valance states is higher than those of all less positive and neutral charge states. For O vacancy in $NaBiO_3$, **Fig. S2** (e2) shows that the formation energy in the +3 charge states is higher than these of all less positive charge states, and the formation energies of all negative charge states are higher than those of positive charge states. Hence, the lowest formation energy changing curve with Fermi energy in the entire bandgap range is composed of the formation energies in the +2 and 0 charge states. For Na vacancy defect, the formation energy of the -1 valance states is lower than those of all positive and more negative charge states in the whole Fermi energy range in **Fig. S2** (e3). The formation energies of the anti-site defect Bi_{Na} in different chare states as in **Fig. S2** (e4) indicates that the formation energy in the +3 is higher than those of in the +1 and +2 charge states, but the formation energy in the +4 charge states is lower than that in the +2 valance states. Thus, the lowest formation energy changing curve with Femi energy in the entire bandgap range is composed of the formation energies in the +4 and +2 charge states. For O interstitials, **Fig. S2** (e5) displays that the formation energy in the +4 charge is the highest among positive charge states; and for negative charge states, the formation energy increases as the charge state decreases. The lowest formation energy changing curve with Fermi energy in the entire bandgap range is composed of the formation energies in the +3 and 0 charge states. The defect Na interstitial in $NaBiO_3$, **Fig. S2** (e6) presents that the formation energy in the +1 charge states is the lowest among all charge states in the whole Fermi energy range. For the anti-site defect Na_{Bi} in **Fig. S2** (e7), the formation energy increases with the increasing charge state among positive charge states and is higher than that in neutral charge state; for negative charge states, the formation energy in the -4 charge at a given Fermi energy is the highest. For intrinsic Bi interstitial, the formation energy in the +4 charge is higher than those of all positive charge states; and for negative charge states, the formation energy increases as the charge state decreases and is higher than that in the neutral charge state

at a given Fermi energy. The lowest formation energy changing curve with Fermi energy in the entire Fermi level range are composed of the formation energies in the +3 and +2 charge sates.

Note S7: The defect and carrier concentrations as a Function of ΔμNa

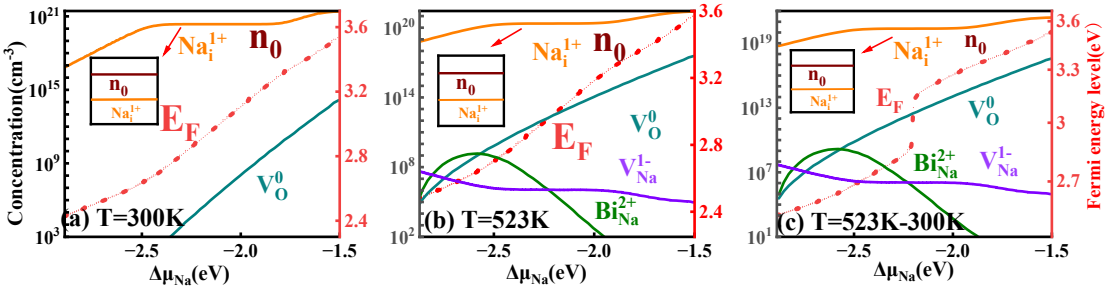

Fig. S3. The calculated concentrations of carriers and major intrinsic defects (solid color line, left axis) in $NaBiO_3$ and the self-consistent Fermi level by HSE method (red dashed line, right axis), taking ΔμNa as variable along the $A_{HSE}E_{HSE}C_{HSE}$ curve in **Fig. 2**, (a) 300K and (b) 523K under thermodynamic equilibrium conditions; and (c) when the temperature is quenched from 523K to 300K under non-thermodynamic equilibrium conditions.

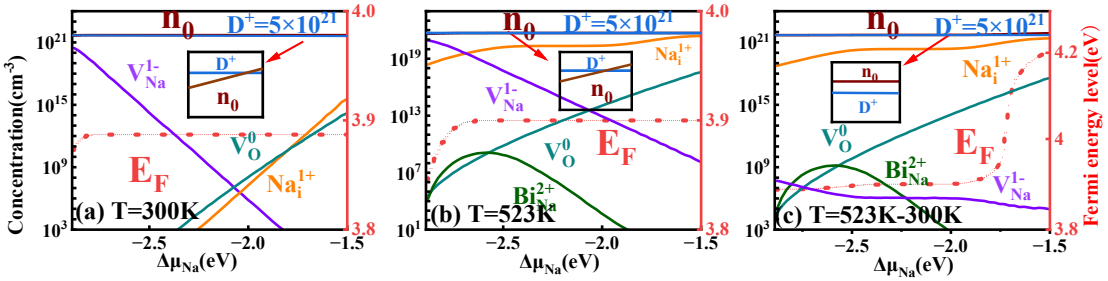

Fig. S4. Under the fixed extrinsic donor doping concentration $[D^+] = 5\times10^{21}$ cm^{-3}, the calculated concentrations of carriers and major intrinsic defects (solid color line, left axis) in $NaBiO_3$ and the self-consistent Fermi level by HSE method (red dashed line, right axis), taking ΔμNa as variable along the $A_{HSE}E_{HSE}C_{HSE}$ curve in **Fig. 2**, (a) 300K and (b) 523K under thermodynamic equilibrium conditions; and (c) when the temperature is quenched from 523K to 300K under non-thermodynamic equilibrium conditions.

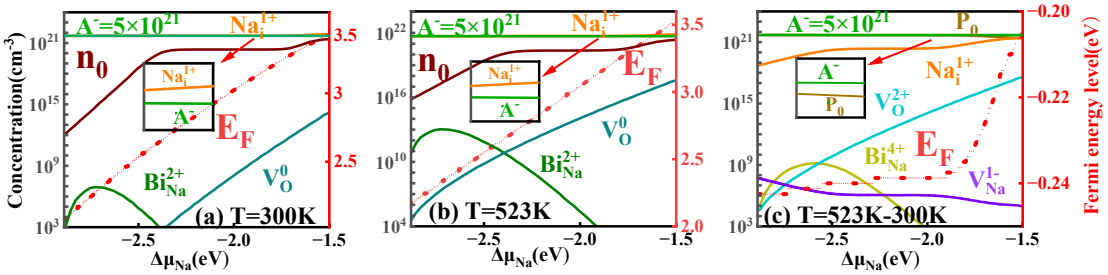

Fig. S5. Under the fixed extrinsic acceptor doping concentration $[A^-] = 5\times10^{21}$ cm−3, the calculated concentrations of carriers and major intrinsic defects (solid color line, left axis) in $NaBiO_3$ and the self-consistent Fermi level by HSE method (red dashed line, right axis), taking ΔμNa as variable along the $A_{HSE}E_{HSE}C_{HSE}$ curve in **Fig. 2**, (a) 300K and (b) 523K under thermodynamic equilibrium

conditions; and (c) when the temperature is quenched from 523K to 300K under non-thermodynamic equilibrium conditions.

References

1. H. Peelaers, J. L. Lyons, J. B. Varley and C. G. Van de Walle, *APL Materials*, 2019, **7**, 022519.
2. S. Mu, M. Wang, J. B. Varley, J. L. Lyons, D. Wickramaratne and C. G. Van de Walle, *Physical Review B*, 2022, **105**,155201.
3. W. Ming, H. Shi and M.-H. Du, *Journal of Materials Chemistry A*, 2016, **4**, 13852-13858.
4. J. Buckeridge, T. D. Veal, C. R. A. Catlow and D. O. Scanlon, *Physical Review B*, 2019, **100**, 035207.
5. S. R. Kavanagh, A. Walsh and D. O. Scanlon, *ACS Energy Lett.*, 2021, **6**, 1392-1398.
6. T. Kako, Z. Zou, M. Katagiri and J. Ye, *Chem. Mater*, 2006, **19**, 198-202.
7. C. Freysoldt, J. Neugebauer and C. G. Van de Walle, *Phys Rev Lett* 2009, **102**, 016402.
8. J. Buckeridge, *Comput. Phys. Commun.*, 2019, **244**, 329-342.
9. J. Buckeridge, T. Veal, C. Catlow and D. Scanlon, *Phys. Rev. B*, 2019, **100**, 035207.
10. L. Weston, L. Bjaalie, K. Krishnaswamy and C. Van de Walle, *Phys. Rev. B*, 2018, **97**, 054112.
11. F. Ren, J. Zhang, Y. Wang and W. Yao, *Phys. Chem. Chem. Phys.*, 2016, **18**, 14113-14121.
12. V. Wang, N. Xu, J. C. Liu, G. Tang and W. T. Geng, *Comput. Phys. Commun.*, 2021, **267**, 108033.